WARSAW UNIVERSITY OF TECHNOLOGY Index 351733
FACULTY OF CIVIL ENGINEERING
COMMITTEE FOR CIVIL AND WATER ENGINEERING
POLISH ACADEMY OF SCIENCES ISSN 1230-2945

DOI: 10.24425/ace.2023.144178

ARCHIVES OF CIVIL ENGINEERING

Vol. LXIX ISSUE 1 2023

pp. 367 –384

Research paper

Bearing capacity and seismic performance of Y-shaped reinforced concrete bridge piers in a freeze-thaw environment

Yanfeng Li[1], Jialong Li[2], Tianyu Guo[3], Tongfeng Zhao[4], Longsheng Bao[5], Xinglong Sun[6]

Abstract: A quantitative study is performed to determine the performance degradation of Y-shaped reinforced concrete bridge piers owing to long-term freeze-thaw damage. The piers are discretized into spatial solid elements using the ANSYS Workbench finite element analysis software, and a spatial model is established. The analysis addresses the mechanical performance of the piers under monotonic loading, and their seismic performance under low-cycle repeated loading. The influence of the number of freeze-thaw cycles, axial compression ratio, and loading direction on the pier bearing capacity index and seismic performance index is investigated. The results show that freeze-thaw damage has an adverse effect on the ultimate bearing capacity and seismic performance of Y-shaped bridge piers in the transverse and longitudinal directions. The pier peak load and displacement ductility coefficient decrease with increasing number of freeze-thaw cycles. The axial compression ratio is an important factor that affects the pier ultimate bearing capacity and seismic performance. Upon increasing the axial compression ratio, the pier peak load increases and the displacement ductility coefficient decreases, the effects of which are more significant in the longitudinal direction.

Keywords: freeze-thaw cycle, Y-shaped bridge pier, finite element analysis, bearing capacity, seismic resistance

[1]Prof., PhD., School of Transportation and Geomatics Engineering, Shenyang Jianzhu University, Shenyang 110168, China, e-mail: lyfneu@126.com, ORCID: 0000-0003-2153-7934
[2]MEng., School of Transportation and Geomatics Engineering, Shenyang Jianzhu University, Shenyang 110168, China, e-mail: lijialong@stu.sjzu.edu.cn, ORCID: 0000-0001-9343-1501
[3]MEng., School of Transportation and Geomatics Engineering, Shenyang Jianzhu University, Shenyang 110168, China, e-mail: gtyarron@126.com, ORCID: 0000-0003-4945-5770
[4]Prof., PhD., Liaoning Provincial College of Communications, Liaoning Bridge Safety Engineering Research Center, Shenyang 110168, China, e-mail: 734849351@qq.com, ORCID: 0000-0001-6504-781X
[5]Prof., PhD., School of Transportation Engineering, Shenyang Jianzhu University, Shenyang 110168, China, e-mail: 13516094255@163.com, ORCID: 0000-0001-5582-1103
[6]MEng., School of Transportation and Geomatics Engineering, Shenyang Jianzhu University, Shenyang 110168, China, e-mail: sxl0660@163.com, ORCID: 0000-0002-9965-2505

1. Introduction

Rapid economic development and accelerated urbanization in China have led to the widespread use of Y-shaped bridge piers in urban viaducts owing to their attractive appearance and strong adaptability. Y-shaped piers are bifurcated in their upper and middle parts to form two limbs, and their force characteristics are more complicated than straight piers. Y-shaped piers have been extensively studied [1–8]. For example, Yan et al. used spatial and deep beam calculation models to analyze the mechanical effects of Y-shaped piers of the Wangjiahe Bridge on Yueyang Avenue (Yanchixiang, Shanxi Province, China) under extreme conditions, and studied the influence of pier height and reinforcement using three-dimensional finite element numerical simulation analysis [9]. Zhang proposed that the structural characteristics of the two Y-shaped bridge pier limbs affect the force transmission path and concentrate the tensile stress on the two supports on the top of the pier, and designed the pier section reinforcement ratio according to the tensile stress cloud diagram obtained from three-dimensional elastic analysis [10]. Zhou used a spatial finite element model to analyze the influence of the central beam on the force of a Y-shaped pier, and reported that the pier lateral force can be improved by setting the central beam with prestressed steel bars [11]. Fan studied the force characteristics of the split section of the Y-shaped pier of the Qinglian Expressway viaduct (lianzhou, Guangdong Province, China) using numerical simulation methods, and analyzed the influence of the reinforcement ratio on the pier force [12].

Numerous studies have addressed the optimization design, applicable conditions, calculation and reinforcement methods, beam performance, and seismic performance of Y-shaped bridge piers under normal atmospheric temperature conditions. However, concrete in certain cold and severely cold regions can be damaged by freeze-thaw cycles, particularly in areas where an average of 80 freeze-thaw cycles occur per year [13–16]. The long-term effects of repeated freeze-thaw cycles strongly reduce the frost resistance durability of Y-shaped bridge piers in such environments. The microscopic manifestation of freeze-thaw damage includes the generation or rapid development of internal cracks, whereas the macroscopic manifestation includes the peeling and chipping of the outer component layer, which strongly damages the structure or component and is an important factor that affects its overall durability [17–21]. The continuous accumulation of such damage over time degrades the pier structural bearing capacity and seismic performance [22–25]. Numerical simulation analyses of Y-shaped piers with existing durability damage are therefore important to objectively manage such processes and develop methods for damage mitigation. However, the impact of durability damage on Y-shaped bridge piers under freeze-thaw environments remains poorly understood. Comprehensive studies on the bearing capacity and seismic performance of Y-shaped bridge piers, which are widely used in urban viaducts and overpasses, after freeze-thaw damage therefore offer important theoretical guidance and engineering value. This paper based on the ANSYS Workbench software, a finite element model of the Y-shaped pier of the urban viaduct was established, which can provide a reference for the researchers in the numerical simulation. According to the actual engineering background, combined with the research results of this paper, which can provide a reference for the design of Y-shaped piers damaged by long-term freeze-thaw in severe cold areas.

2. Research background

The Y-shaped viaduct pier of a certain city is taken as the engineering background. The temperature change of the city where the Y-shaped pier is located is: the annual average temperature is –12° (January) and 24.6° (July).The Y-shaped pier is 9-m high and uses C40 concrete. The dimensions of the rectangular section of the two pier limbs are 160 × 190 cm, and the vertical bending radius is 1500 cm. The four corners of the limb section are rounded with a radius of 15 cm, and the middle of both sides is set with a 23 × 18 cm drainage channel. A horizontal connecting beam is set 30 cm below the top of the pier with dimensions of 80 × 130 cm. A U-shaped groove with a radius of 70 cm is set 440 cm below the top of the pier. The lower connecting components between the two limb arms are set beneath the U-shaped groove with a width of 120 cm in the transverse bridge and 130 cm in the longitudinal bridge. The dumbbell-shaped cross-section formed by the two arms and lower connection component is under the U-shaped groove, and has dimensions of 160 × 500 cm. The ordinary steel bars are HRB400 hot-rolled ribbed steel bars, and the cross beam prestressed steel bars are JL32 fine-rolled rebars. C12 stirrups are used for the two limb arms, and the 20-cm area of the top and bottom of the pier is densely arranged. C32 longitudinal reinforcement is adopted in the transverse direction and C28 longitudinal reinforcement is adopted in the longitudinal direction. The cross beams are positioned in a staggered arrangement of C32 ordinary steel bars and JL32 prestressed steel bars. The prestress is applied by single-end tensioning. The U-shaped groove area is densely arranged with C12U-shaped steel bars and C16 structural straight bars. The lower connection between the two limbs adopts C20 longitudinal reinforcement, C20 structural straight reinforcement, and C16 stirrups. The layout of cross-sectional reinforcement is shown in Fig. 1.

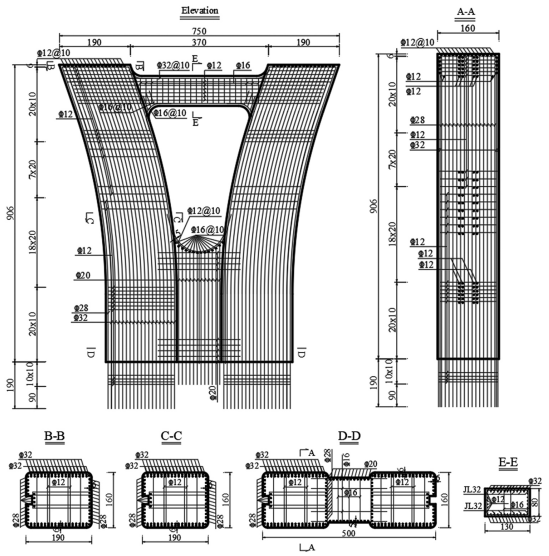

Fig. 1. Rebar layout drawing of a Y-shaped bridge pier section (unit: cm)

3. Establishment of a finite element model of a y-shaped reinforced concrete pier damaged by freezing and thawing

ANSYS Workbench finite element software is used to establish a separated space finite element model of Y-shaped reinforced concrete piers after freeze-thaw damage. The pier concrete adopts eight-node SOLID 65 three-dimensional solid elements, and the reinforcement adopts two-node LINK8 three-dimensional bar elements. The model has a total of 80,047 nodes, 73113 elements, 71,600 concrete elements, and 1513 steel reinforcement elements. In the Connect module, set the contact mode as Bonded, it is assumed that the bond behavior between reinforcement and concrete is good without relative slip. In the Model module, material properties are assigned to the geometric structure, and the fixed support boundary of the pier bottom are set.The concrete model and steel cage model are shown in Fig. 2a and Fig. 2b.

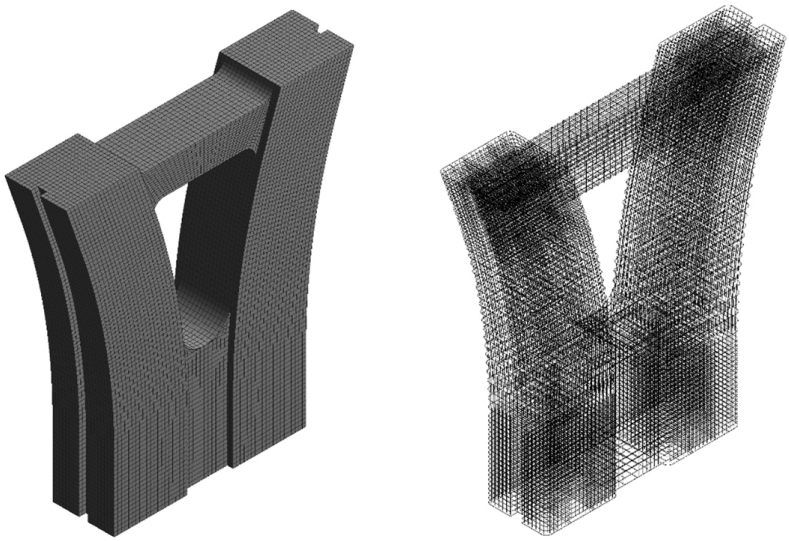

(a) Bridge pier concrete (b) Steel cage

Fig. 2. Finite element model of a Y-shaped pier

The reinforcement material adopts the bilinear follow-up strengthening criterion, and defines its constitutive relationship using a two broken line model. The yield stress during the yield stage reaches 400 MPa, and the tangent modulus in the strengthening stage is 2000 MPa.

The concrete material adopts the multi-linear isotropic strengthening criterion, which is based on the piecewise equation of the concrete compressive stress-strain curve proposed by Guo [25]. The polynomial regression method is used in SPSS software to regress the

equation parameters. The analysis allows a constitutive model of freeze-thaw damaged concrete to be established under compression and tension conditions, and the damage evolution parameters are determined to assess the extent of concrete damage. This article takes the piecewise equation of the concrete compressive stress-strain curve:

$$y = \frac{\sigma}{f_c^d} \begin{cases} a_a^d \left(3 - 2a_a^d\right) x^2 + \left(a_a^d - 2\right) x^3 & x = \dfrac{\varepsilon}{\varepsilon_c^d} \le 1 \\ \dfrac{x}{a_b^d (x-1)^2 + x} & x = \dfrac{\varepsilon}{\varepsilon_c^d} \ge 1 \end{cases} \tag{3.1}$$

where: f_c^d – peak compressive stress of concrete after freeze-thaw cycle, ε_c^d – Peak compressive strain of freeze-thaw cycle, a_a^d – rising parameter of concrete after freeze-thaw cycle, a_b^d – descending parameter of concrete after freeze-thaw cycle.

This article takes the piecewise equation of the concrete tensile stress-strain curve:

$$y = \frac{\sigma}{f_t^d} \begin{cases} 1.2x - 0.2x^6 & x = \dfrac{\varepsilon}{\varepsilon_t^d} \le 1 \\ \dfrac{x}{a_t^d (x-1)^{1.7} + x} & x = \dfrac{\varepsilon}{\varepsilon_t^d} \ge 1 \end{cases} \tag{3.2}$$

where: f_t^d – peak tensile stress of concrete after freeze-thaw cycle, ε_t^d – peak tensile strain of freeze-thaw cycle, a_t^d – the descending parameter of concrete after freeze-thaw cycle.

The full compression and tension stress-strain curves of C40 concrete are shown in Fig. 3a and Fig. 3b. The calculation parameters of concrete tensile and compression behavior are shown in Table 1 and Table 2.

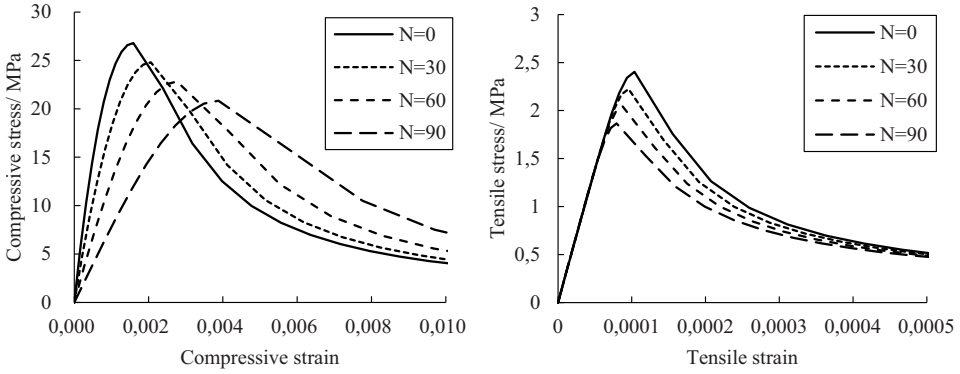

(a) Compressive stress-strain curve (b) Tensile stress-strain curve

Fig. 3. Stress-strain curve model of C40 concrete after freeze-thaw cycles

Table 1. Calculation parameters of C40 concrete tensile behavior

N 0		N 30		N 60		N 90	
Yield Stress (MPa)	Cracking Strain	Yield Stress (MPa)	Cracking Strain	Yield Stress (MPa)	Cracking Strain	Yield Stress (MPa)	Cracking Strain
0.28846	0.00000	0.26462	0.00000	0.24079	0.00000	0.21698	0.00000
0.57690	0.00002	0.52922	0.00002	0.48156	0.00002	0.43393	0.00002
0.86504	0.00003	0.79355	0.00003	0.72209	0.00003	0.65067	0.00002
1.15188	0.00004	1.05669	0.00004	0.96153	0.00003	0.86643	0.00003
1.43481	0.00005	1.31623	0.00005	1.19770	0.00004	1.07924	0.00004
1.70835	0.00006	1.56716	0.00006	1.42604	0.00005	1.28499	0.00005
1.96268	0.00007	1.80048	0.00007	1.63835	0.00006	1.47630	0.00005
2.18168	0.00008	2.00137	0.00008	1.82115	0.00007	1.64102	0.00006
2.34067	0.00009	2.14723	0.00009	1.95387	0.00008	1.76061	0.00007
2.40386	0.00010	2.20520	0.00010	2.00662	0.00009	1.80815	0.00008
1.75472	0.00016	1.68166	0.00014	1.59537	0.00013	1.49519	0.00012
1.26422	0.00021	1.25394	0.00019	1.23246	0.00017	1.19743	0.00015
0.98649	0.00026	0.99823	0.00024	1.00273	0.00022	0.99738	0.00019
0.81416	0.00031	0.83430	0.00029	0.85006	0.00026	0.85909	0.00023
0.69764	0.00036	0.72109	0.00033	0.74204	0.00030	0.75854	0.00027
0.61361	0.00042	0.63822	0.00038	0.66160	0.00034	0.68214	0.00031
0.55004	0.00047	0.57482	0.00043	0.59926	0.00039	0.62202	0.00035
0.50015	0.00052	0.52465	0.00048	0.54942	0.00043	0.57337	0.00039
0.45986	0.00057	0.48386	0.00052	0.50856	0.00047	0.53310	0.00042
0.42658	0.00062	0.44997	0.00057	0.47439	0.00052	0.49914	0.00046
0.37463	0.00073	0.39674	0.00067	0.42029	0.00060	0.44485	0.00054
0.33576	0.00083	0.35662	0.00076	0.37918	0.00069	0.40316	0.00062
0.30543	0.00094	0.32517	0.00086	0.34672	0.00077	0.36998	0.00069
0.28102	0.00104	0.29974	0.00095	0.32035	0.00086	0.34284	0.00077
0.20593	0.00156	0.22092	0.00143	0.23783	0.00129	0.25688	0.00116

Table 2. Calculation parameters of C40 concrete compression behavior

N 0		N 30		N 60		N 90	
Yield Stress (MPa)	Inelastic Strain	Yield Stress (MPa)	Inelastic Strain	Yield Stress (MPa)	Inelastic Strain	Yield Stress (MPa)	Inelastic Strain
4.60943	0.00000	4.62981	0.00000	4.66398	0.00000	4.71605	0.00000
8.88541	0.00033	8.75909	0.00057	8.65455	0.00081	8.57830	0.00105
12.79222	0.00050	12.39095	0.00085	12.01469	0.00121	11.67091	0.00157
16.29409	0.00066	15.52848	0.00114	14.78737	0.00162	14.07808	0.00209
19.35529	0.00083	18.17479	0.00142	17.01557	0.00202	15.88396	0.00262
21.94006	0.00099	20.33300	0.00171	18.74226	0.00242	17.17275	0.00314
24.01266	0.00116	22.00619	0.00199	20.01044	0.00283	18.02861	0.00366
25.53735	0.00132	23.19749	0.00228	20.86307	0.00323	18.53572	0.00418
26.47838	0.00149	23.90999	0.00256	21.34313	0.00363	18.77826	0.00471
26.80000	0.00165	24.14680	0.00285	21.49360	0.00404	18.84040	0.00523
22.36813	0.00248	19.11659	0.00427	16.18331	0.00606	13.52376	0.00785
16.80883	0.00331	13.49436	0.00569	10.83128	0.00808	8.64476	0.01046
12.94736	0.00413	9.97422	0.00712	7.75405	0.01010	6.03294	0.01308
10.36724	0.00496	7.77658	0.00854	5.92916	0.01212	4.54526	0.01569
8.58188	0.00579	6.32233	0.00996	4.75973	0.01414	3.61471	0.01831
7.29291	0.00661	5.30431	0.01138	3.95845	0.01615	2.98708	0.02092
6.32646	0.00744	4.55785	0.01281	3.37976	0.01817	2.53873	0.02354
5.57850	0.00827	3.98978	0.01423	2.94426	0.02019	2.20403	0.02616
4.98424	0.00909	3.54430	0.01565	2.60568	0.02221	1.94538	0.02877
4.50168	0.00992	3.18629	0.01708	2.33541	0.02423	1.73992	0.03139
3.76731	0.01158	2.64781	0.01992	1.93196	0.02827	1.43481	0.03662
3.23617	0.01323	2.26302	0.02277	1.64590	0.03231	1.21963	0.04185
2.83487	0.01488	1.97487	0.02561	1.43287	0.03635	1.06002	0.04708
2.52134	0.01654	1.75126	0.02846	1.26826	0.04039	0.93704	0.05231
1.62094	0.02480	1.11637	0.04269	0.80423	0.06058	0.59206	0.07847

4. Degradation analysis of the bridge pier bearing capacity under monotonic loading in a freeze-thaw environment

The stress-strain curves of the concrete after freeze-thaw cycling present the following information. The damage of the concrete specimen is more notable after 90 freeze-thaw cycle than the specimen that has not been subjected to freeze-thaw cycling. For comparison and analysis purposes, finite element numerical simulations are performed on Y-shaped C40 concrete piers that undergo 0, 30, 60, and 90 freeze-thaw cycles for two axial compression ratio (μ) values of 0.2 and 0.4. The analysis of the mechanical performance of each parameter is based on the load-displacement curve of the pier model after monotonic loading. Following the results presented in Cao et al [27,28], this paper simulates Y-shaped bridge piers after 90 indoor freeze-thaw cycles on the basis of the concrete constitutive relationship obtained from fast-freezing and quick-thaw indoor test data. It is equivalent to 1080 freeze-thaw cycles in 9 years under natural conditions in Northeast China.

4.1. Analysis of the impact of freeze-thaw damage

Figure 4 shows the load-displacement curves of the Y-shaped piers after different numbers of freeze-thaw cycles (N) for an axial compression ratio of μ = 0.2. The results indicate that the peak load in the longitudinal direction of the bridge decreases from 4337.22 N prior to freeze-thaw action to 4252.10, 4106.87, and 3939.89 kN after 30, 60, and 90 freeze-thaw cycles, respectively, reflecting a decrease of 1.96%, 5.31%, and 9.16%. Similarly, the peak load in the transverse direction decreases from 7707.72 kN prior to freeze-thaw action to 7607.94, 7301.66, and 6955.92 kN after 30, 60, and 90 freeze-thaw cycles, respectively; a decrease of 1.29%, 5.27%, and 9.75%.

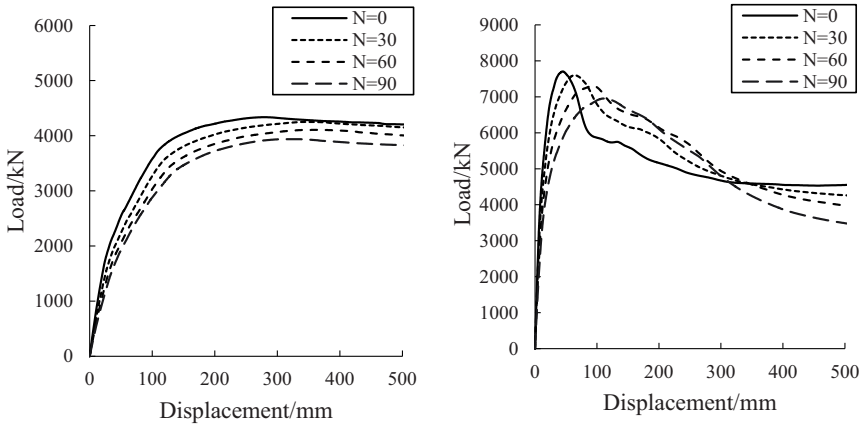

(a) Load in the longitudinal direction (b) Load in the transverse direction

Fig. 4. Load-displacement curve of Y-shaped piers under monotonic loading (μ = 0.2)

The freeze-thaw damage from the surface to the interior continuously deepens with increasing N. This degrades not only the physical performance parameters of the concrete materials, but also their macro-mechanical properties. Freeze-thaw damage has an adverse effect on the ultimate bearing capacity of Y-shaped bridge piers in the longitudinal and transverse directions. For models with the same μ value, the peak load of the pier load-displacement curve continuously decreases with deepening freeze-thaw damage, and the peak point continuously decreases and shifts to the right.

4.2. Analysis of the influence of axial compression ratio

Figure 5 shows the load-displacement curves of the Y-shaped pier after N freeze-thaw cycles and $\mu = 0.4$. The results indicate that higher μ values enhance the peak load along the bridge and transverse bridge directions to 5302.21 and 8716.67 kN, respectively, for the Y-shaped pier that is monotonically loaded but not treated to freeze-thaw action; reflecting an increase of 22.25% and 13.09%, respectively.

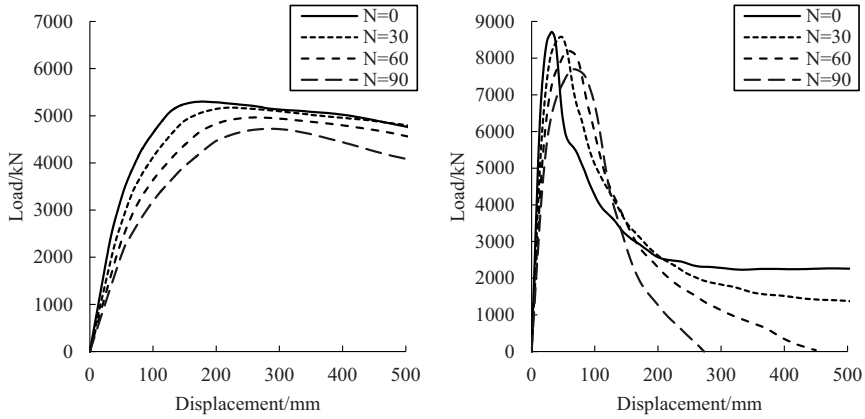

(a) Longitudinal direction (b) Transverse direction

Fig. 5. Load-displacement curves of Y-shaped piers under monotonic loading ($\mu = 0.4$)

The μ value is thus an important factor that affects the ultimate bearing capacity of Y-shaped piers. Higher μ values increase the peak load Y-shaped piers in both the longitudinal and transverse directions, but the effect is more significant in the former.

Figure 6 shows the peak load changes of the Y-shaped piers with different μ values under monotonic loading due to freezing and thawing. The results indicate that for $N = 90$ and $\mu = 0.2$, the monotonically loaded Y-shaped pier exhibits reduced peak loading rates in the longitudinal and transverse directions by 9.16% and 9.75%, respectively, which increase to 10.87% and 11.65% when $\mu = 0.4$; reflecting an increase of 1.71% and 1.90%.

The frost resistance durability of Y-shaped piers decreases with μ, whereas the peak load reduction rate after freeze-thaw damage increases in both the longitudinal or transverse

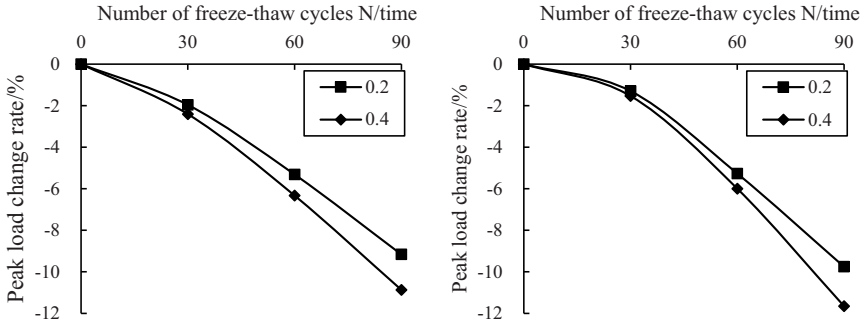

(a) Peak load change in the longitudinal bridge direction

(b) Peak load change in the transverse bridge direction

Fig. 6. Peak load changes of Y-shaped piers with different axial compression ratios

directions. Higher μ values are therefore associated with a faster reduction of the pier bearing capacity under the same freeze-thaw conditions.

4.3. Analysis of different concrete strengths

Comparison of peak loads of different concrete strengths with $\mu = 0.2$ shown in Fig. 7 and Fig. 8.

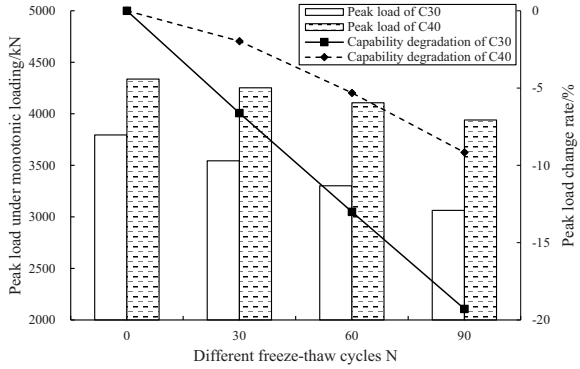

Fig. 7. Comparison of peak loads of different concrete strengths with $\mu = 0.2$ (CIS bridge direction)

It can be seen from Figure 7 that when the C30 Y-shaped pier model, after 90 freeze-thaw cycles, the Y-shaped pier monotonically loads the peak load reduction rates in the longitudinal and transverse directions of 19.28% and 13.25%.

It can be seen from Figure 8 that when the C40 Y-shaped pier model, after 90 freeze-thaw cycles, the Y-shaped pier monotonically loads the peak load reduction rates in the longitudinal and transverse directions of 19.16% and 9.75%.

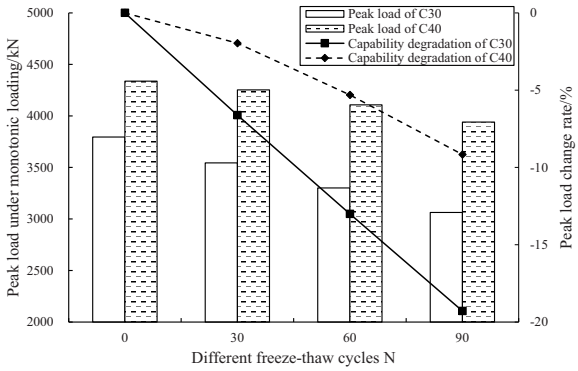

Fig. 8. Comparison of peak loads of different concrete strengths with $\mu = 0.2$ (Cross bridge direction)

Above all, whether in the longitudinal or transverse direction, increasing the concrete strengths increase the frost resistance durability of the Y-shaped pier, the degradation trend of bearing capacity of Y-shaped pier is going to be flat after freezing and thawing cycles, it is conducive to improving the bearing capacity of piers damaged by long-term freeze-thaw.

5. Seismic performance analysis of y-shaped bridge piers in a freeze-thaw environment

Figures 4 and 5 show the $P - \Delta$ load-displacement curve diagrams of the Y-shaped bridge piers under monotonic loading based on the R. PARK method. The yield and ultimate displacement of the Y-shaped pier are determined. The axial pressure is divided into two equal forces and uniformly applied to the top of the two limbs of the Y-shaped pier, and repeated horizontal loads are then applied to the top of the pier. The loading rate remains constant during the loading process until the pier reaches the input limit displacement, or the finite element calculation result does not converge (i.e., the pier is completely destroyed) and the simulation ends. The loading system is shown in Fig. 9.

The model numbers are listed in Table 3, where 0.2/0.4 represents μ, 0/30/60/90 represents N, and S/H represents the loading direction.

Table 3. Model number

Loading direction	Model number			
Longitudinal direction	0.2-0-S	0.2-30-S	0.2-60-S	0.2-90-S
	0.4-0-S	0.4-30-S	0.4-60-S	0.4-90-S
Transverse direction	0.2-0-H	0.2-30-H	0.2-60-H	0.2-90-H
	0.4-0-H	0.4-30-H	0.4-60-H	0.4-90-H

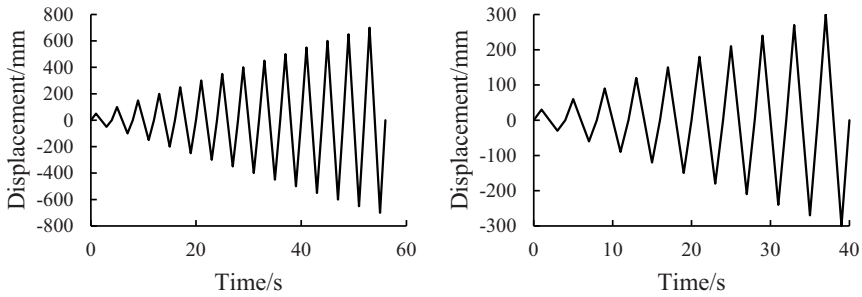

(a) Longitudinal direction (b) Transverse direction

Fig. 9. Seismic performance analysis of the loading system

5.1. Hysteresis curve analysis

Numerical simulations were performed to obtain the hysteretic curve of the pier bottom load and horizontal displacement of the pier top of the bridge pier model. To avoid unnecessary repetition, some representative hysteretic curves are selected for further study, as shown in Fig. 10.

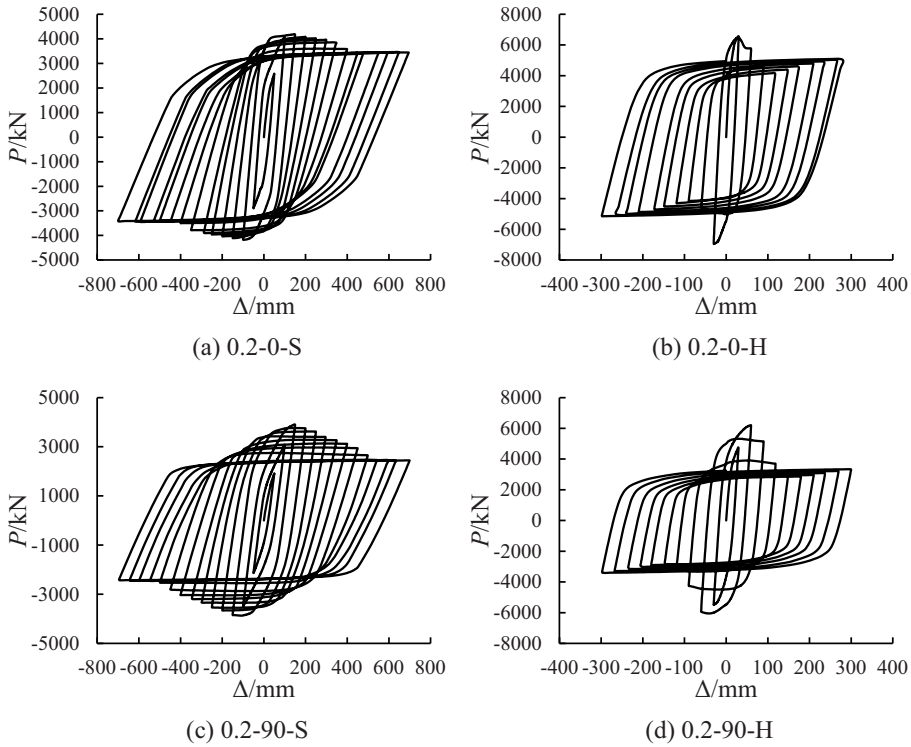

(a) 0.2-0-S (b) 0.2-0-H

(c) 0.2-90-S (d) 0.2-90-H

Fig. 10. Y-shaped pier hysteresis curve

Freeze-thaw damage is found to affect the shape of the hysteresis curve of Y-shaped piers. For a given μ, the plump and stable "shuttle" shape gradually flattens with increasing N, and the number of hysteresis loops continues to decrease. Especially once N reaches 90, the number of model hysteresis loops sharply decreases, the hysteresis curve stability significantly drops after the peak horizontal load, and the damage becomes more abrupt. This demonstrates that the internal damage of the bridge pier continues to accumulate with increasing N and reaches a certain level after which its plastic deformation and energy dissipation characteristics rapidly decline.

5.2. Skeleton curve analysis

For a more intuitive presentation, we take the skeleton curves with $N = 0$ and $N = 90$ for analysis. The influence of freeze-thaw damage on the skeleton curves is shown in Fig. 11 for $\mu = 0.2$.

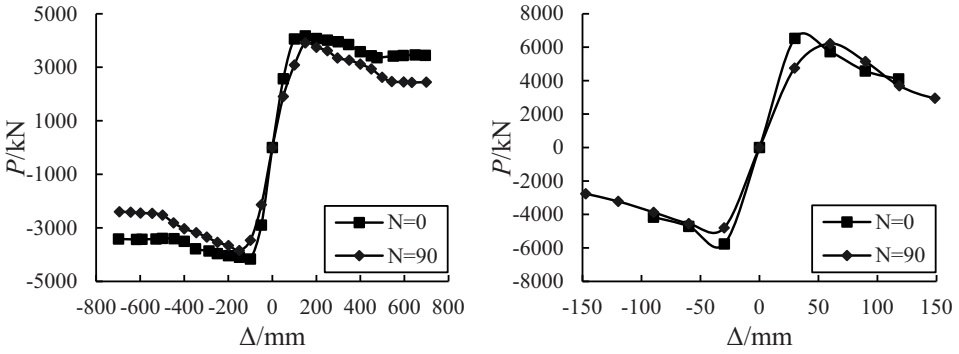

(a) Longitudinal direction (b) Transverse direction

Fig. 11. Influence of the number of freeze-thaw cycles on the skeleton curves of Y-shaped bridge piers ($\mu = 0.2$)

Figure 11 shows that for a given μ value, the peak point of the pier with $N = 90$ is significantly lower and shifted to the right compared with the Y-shaped pier with $N = 0$, and the descending section of the skeleton curve becomes steeper. This shows that the cumulative damage caused by 90 freeze-thaw cycles reduces the ultimate bearing capacity and ductility of the Y-shaped bridge pier, and weakens its seismic resistance. The descending section of the skeleton curve in the longitudinal direction is more gentle than that in the transverse direction, indicating that the Y-shaped pier has a better seismic performance in the longitudinal direction.

Figure 12 shows the skeleton curves of the Y-shaped piers with $N = 90$ and different μ values. After 90 freeze-thaw cycles, the peak load of the pier with $\mu = 0.4$ is higher than that with $\mu = 0.2$, but the peak displacement is smaller and the descending section of the skeleton curve is steeper. This shows that higher μ values increase the ultimate bearing

capacity of Y-shaped piers under a given set of conditions when the other parameters are held fixed, but reduces its plastic deformation capacity and ductility.

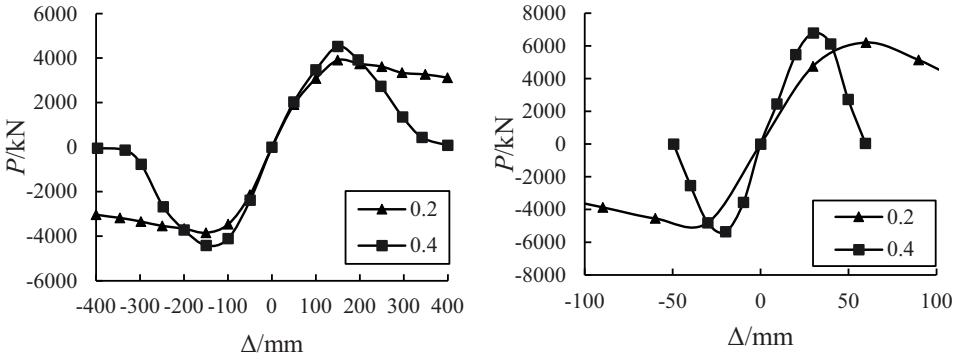

(a) Longitudinal direction (b) Transverse direction

Fig. 12. Influence of axial compression ratio on the skeleton curve of Y-shaped piers (N = 90)

5.3. Displacement ductility analysis

The equivalent elastic-plastic energy method is used to determine the yield displacement on the skeleton curve and corresponding yield load for the case when the peak load drops by 15% as the ultimate displacement. The change of the displacement ductility coefficient for variable μ is shown in Fig. 13. The displacement ductility coefficient of the Y-shaped pier continually decreases with increasing N. This shows that freeze-thaw damage accelerates the brittleness of bridge piers, thus the bearing capacity rapidly drops, the ultimate displacement decreases, and the ductility worsens after yielding and reaching the peak load. The displacement ductility coefficient of Y-shaped piers is larger in the

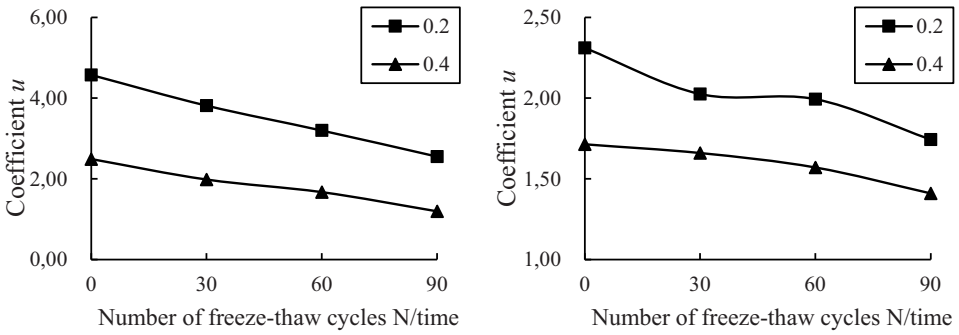

(a) Longitudinal direction (b) Transverse direction

Fig. 13. Influence of the axial compression ratio on the displacement ductility coefficient of Y-shaped bridge piers

longitudinal direction than in the transverse direction, which indicates that Y-shaped piers have a stronger ability to absorb seismic energy in the bridge direction.

When μ is increased from 0.2 to 0.4, the ductility coefficients decreases by 39.05%, 48.03%, 47.72%, and 53.15% after 0, 30, 60 and 90 freeze-thaw cycles, respectively, in the longitudinal bridge direction, and by 25.84%, 18.05%, 21.20%, and 19.11% in the transverse bridge direction. This indicates that the principal compressive stress and corresponding principal compressive strain of the concrete at the edge of the section increase more rapidly for piers with higher μ, which weakens their later concrete deformation capacity. For piers with $\mu = 0.4$, the additional bending moment and additional deformation caused by the axial force more rapidly increase with increasing horizontal displacement. The attenuation of the bridge pier bearing capacity during later deformation is therefore accelerated and difficult to stabilize, and the ductility is poor.

5.4. Stiffness degradation analysis

Figure 10 shows the hysteresis curve of the Y-shaped bridge piers with different N. The bridge pier stiffness is found to continuously degrade with increasing loading displacement. In this paper, the average secant stiffness K_i is used to evaluate the stiffness degradation of the Y-shaped bridge piers for different μ and concrete strength conditions after freeze-thaw damage. The calculation formula of the average secant stiffness K_1 of the loading displacement at all levels is given as:

$$K_{\mathrm{i}} = \frac{|+P_{\mathrm{i}}| + |-P_{\mathrm{i}}|}{|+\Delta_{\mathrm{i}}| + |-\Delta_{\mathrm{i}}|} \tag{5.1}$$

where: $+P_i$ and $-P_i$ – peak load of the i^{th} level of forward and reverse loading (kN), $+\Delta_i$ and $-\Delta_i$ – peak displacement of the i^{th} level of forward and reverse loading (mm).

For comparative analysis, K1/K0 represents the ratio of the normalized average secant stiffness K_1 of each loading displacement to the initial elastic stiffness K0. Fig. 14 shows the K_1/K_0 degradation curve with loading displacement due to the different freeze-thaw cycles when $\mu = 0.2$, which reflects the influence of freeze-thaw damage on the skeleton curve.

Figure 14 shows that freeze-thaw damage affects the stiffness degradation of Y-shaped piers. The stiffness of Y-shaped piers with $N = 90$ degrades significantly faster than that of piers with $N = 0$. This demonstrates that cracks form and/or rapidly develop in bridge piers owing to the effects of freeze-thaw cycles. The effective working area of the bridge piers continues to decrease with increasing load, which results in the continuous stiffness degradation.

The stiffness degradation curves of the Y-shaped piers for different μ values and $N = 90$ are shown in Fig. 15. The Y-shaped bridge pier has a slower degradation rate along the bridge direction than the transverse direction, which indicates a higher energy dissipation capacity in the longitudinal direction and better seismic performance. For a given N value, the Y-shaped pier with $\mu = 0.4$ degrades faster than that with $\mu = 0.2$. This shows that

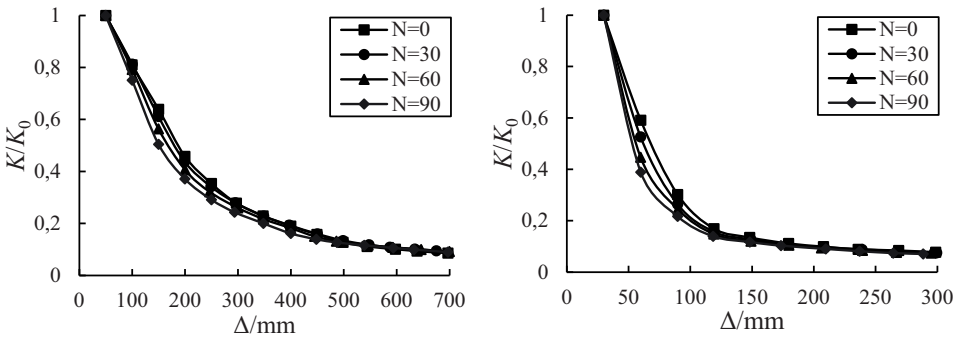

(a) Longitudinal direction (b) Transverse direction

Fig. 14. Influence of the number of freeze-thaw cycles on the stiffness degradation

during an earthquake, internal cracks develop faster in piers with higher μ and the seismic performance degrades more rapidly.

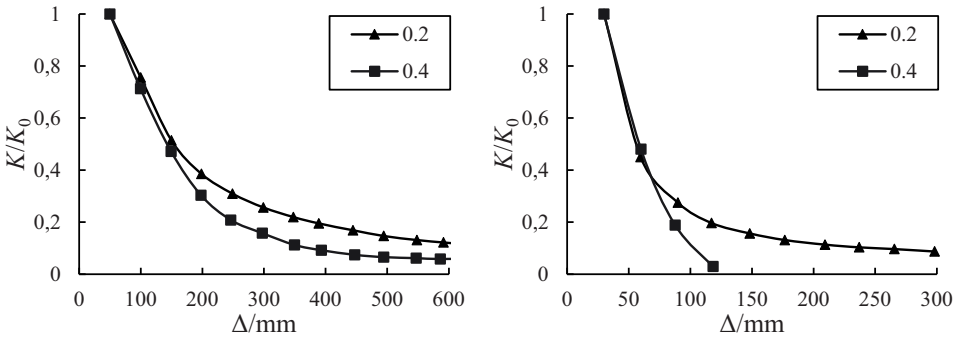

(a) Longitudinal direction (b) Transverse direction

Fig. 15. Influence of axial compression ratio on the stiffness degradation

6. Conclusions

This paper studies the mechanical performance of Y-shaped piers of urban viaducts damaged by long-term freeze-thaws cycling in severely cold environments under monotonic loading, and their seismic performance under low cyclic loading. A combination of theoretical analysis and numerical simulations are used. The influence of different parameters (e.g., number of freeze-thaw cycles, axial compression ratio, loading direction) on the bearing capacity and seismic performance of the Y-shaped bridge piers is obtained. The conclusions are summarized as follows.

1. Freeze-thaw damage has an adverse effect on the longitudinal and transverse ultimate bearing capacity and seismic performance of Y-shaped bridge piers. The peak load and displacement ductility coefficient of bridge piers decrease with increasing number of freeze-thaw cycles. After 90 freeze-thaw cycles on a C40 pier with an axial compression ratio of 0.2, the longitudinal and transverse peak loads decrease by 9.16% and 9.75%, respectively, and the respective displacement ductility coefficients decrease by 44.24% and 24.57%.
2. Above all, whether in the longitudinal or transverse direction, increasing the concrete strengths increase the frost resistance durability of the Y-shaped pier, the degradation trend of bearing capacity of Y-shaped pier is going to be flat after freezing and thawing cycles, it is conducive to improving the bearing capacity of piers damaged by long-term freeze-thaw.
3. The axial compression ratio is an important factor that affects the ultimate bearing capacity and seismic performance of Y-shaped bridge piers. When the axial compression ratio is less than 0.4, an increase of the axial compression ratio will increase the peak load and reduce the displacement ductility coefficient, and the effect is more significant in the longitudinal direction. Upon increasing the axial compression ratio of a C40 pier that has not been subjected to freeze-thaw action from 0.2 to 0.4, the longitudinal and transverse peak loads increase by 22.25% and 13.09%, respectively, and the displacement ductility coefficients decrease by 39.05% and 25.84%. The peak loads in the longitudinal and transverse directions of the piers subjected to 90 freeze-thaw cycles increase by 19.95% and 10.71%, respectively, and the displacement ductility coefficients decrease by 53.15% and 19.11%.

References

[1] Y.L. Tang, Y.G. Sui, and Z. Min, "Superficial Analysis of Optimization Design of Y-Type Pier of Reinforced Concrete", *BeiFang JiaoTong*, no. 11, pp. 63–64, 2008, DOI: 10.3969/j.issn.1673-6052.2008.11.024.

[2] L.J. Jia, J.T. Huang, and H.B. Hui, "Influence Analysis of Mechanical Properties of Y-Type Pier Rigid-frame Bridge", *Shanghai Highwats*, no. 2, pp. 49–53+13–14, 2008.

[3] Y.M. Jin and J. Ding, "Stress analysis and construction control for Y-shaped pier of the continuous rigid frame bridge", *SHANXI ARCHITECTURE*, vol. 36, no. 25, pp. 305–306, 2010, DOI: 10.3969/j.issn.1009-6825.2010.25.192.

[4] S.T. Fan, "Design and construction at the forked part of the Y-type pier of the bridge", *SHANXI ARCHITECTURE*, vol. 37, no. 21, pp. 188–189, 2011, DOI: 10.3969/j.issn.1009-6825.2011.21.111.

[5] K. Li, Q.F. Wang, and J. Li, "Influence of Y-shape Pier Rigidity Change on Bridge Structure and Countermeasures", *Building Technique Development*, vol. 41, no. 5, pp. 4–6, 2014.

[6] L. Yan and Q.N. Li, "Experimental study on Y-shaped bridge under 3-dimentional earthquake ground motions", *KSCE Journal of Civil Engineering*, vol. 21, no. 6, pp. 2329–2337, 2017, DOI: 10.1007/s12205-016-1039-7.

[7] F. Zareian and H. Krawinkler, "Structural system parameter selection based on collapse potential of buildings in earthquakes", *Journal of Structural Engineering*, vol. 136, no. 8, pp. 933–943, 2010, DOI: 10.1061/(ASCE)ST.1943-541X.0000196.

[8] C.B. Haselton, A.B. Liel, et al., "Seismic collapse safety of reinforced concrete buildings. I: Assessment of ductile moment frames", *Journal of Structural Engineering*, vol. 137, no. 4, pp. 481–491, 2011, DOI: 10.1061/(ASCE)ST.1943-541X.0000318.

[9] X.C. Yan and X.D. Dai, "Y-shaped pier design", *Hunan Communication Science and Technology*, 2003, no. 02, pp. 59–60, 2003, DOI: 10.3969/j.issn.1008-844X.2003.02.026.

[10] L. C. Zhang, "Structural analysis and reinforcement of Y-shaped pier top", *China Municipal Engineering*, no. 06, pp. 22–23+87, 2008, DOI: 10.3969/j.issn.1004-4655.2008.06.010.

[11] C.H. Zhou, "Mechanical characteristics analysis and monitoring strategy of Y-shaped pier of wide cast-in-place box girder", *Gong Lu Jiao Tong Ke Ji*, vol. 44, no. 02, pp. 214–215, 2015.

[12] S.T. Fan, "Design and construction at the forked part of the Y-type pier of the bridge", *Shanxi Architecture*, vol. 37, no. 21, pp. 188–189, 2011, DOI: 10.3969/j.issn.1009-6825.2011.21.111.

[13] Y.F. Li, W.L. Luo, and L. Liang, "Analysis for energy dissipation mechanism of Y type prestressed concrete bridge pier under strong earthquake", *Journal of Shenyang University of Technology*, vol. 40, no. 05, pp. 588–594, 2018, DOI: 10.7688/j.issn.1000-1646.2018.05.19.

[14] Y.F. Li, W.L. Luo, L. Liang, "Seismic performance evaluation of reinforced concrete Y-shaped pier under strong earthquake", *Journal of Shenyang University of Technology*, vol. 42, no. 01, pp. 109–114, 2020, DOI: 10.7688/j.issn.1000-1646.2020.01.20.

[15] J. Y. Li, X. P. Peng, and J. G. Cao, "Quantitative Design on the Frost-resistance of Concrete", in *Proceedings of the 2000: 5th National Symposium on durability of concrete, China,* vol. 134, no. 8, pp. 61–65.

[16] J.H. Liu, "Analysis and Control Measures of the Crack of Y Type Pier for Long Span Continuous Rigid Frame Bridge", *Rigid Frame Bridge*, no. 11, pp. 114–117, 2019, DOI: 10.13616/j.cnki.gcjsysj.2019.06.038.

[17] H. Luan, J. Wu, and J. Pan, "Freeze-thaw durability of recycled aggregate concrete: an overview", *Journal of Wuhan University of Technology-Mater*, vol. 36, no. 1, pp. 58–69, 2021, DOI: 10.1007/s11595-021-2378-x.

[18] X. Deng, Y. Liu, and R. Wang, "Investigating freeze-proof durability of air-entrained C30 recycled coarse aggregate concrete", *Archives of Civil Engineering*, vol. 67, no. 2, pp. 507-524, 2021, DOI: 10.24425/ace.2021.137182.

[19] H.R. Wu, W.L. Jin, et al., "A state-of-the-art review on freeze-thaw damage characteristics of concrete under environmental actions", *China Civil Engineering Journal*, 2008, vol. 51, no. 08, pp. 37–46, 2008, DOI: 10.15951/j.tmgcxb.2018.08.005.

[20] Y.X. Zeng, P.B. Yang, and H.G. Kang, "The Overview of Concrete Structure Durabililty under the Freeze-thaw Condition", *Journal of Zhengzhou University (Engineering Science)*, vol. 37, no. 05, pp. 27–37, 2016, DOI: 10.13705/j.issn.1671-6833.2016.05.006.

[21] D. Liu, Y. Tu, et al., "Freeze-thaw damage evaluation and model creation for concrete exposed to freeze–thaw cycles at early-age", *Construction and Building Materials*, vol. 312, art. no. 125352, 2021, DOI: 10.1016/j.conbuildmat.2021.125352.

[22] Y. Zhang, S. Zheng, et al., "Seismic performance of reinforced concrete short columns subjected to freeze-thaw cycles", *Applied Sciences*, vol. 9, no. 13, art. no. 2708, 2019, DOI: 10.3390/app9132708.

[23] D. Xin, M. Sun, and C Zou, "Simulation and prediction of seismic behaviors for RC columns under freeze–thaw cycles", *Engineering Structures*, vol. 216, art. no. 110787, 2020, DOI: 10.1016/j.engstruct.2020.110787.

[24] S.S. Zheng, Y.X. Zhang, et al., "Experimental research on seismic behavior of reinforced concrete columns subjected to freeze-thaw cycles", *Journal of Building Structures*, vol. 41, no. 06, pp. 84–91, 2020, DOI: 10.14006/j.jzjgxb.2017.0838.

[25] W. Tian, Y.L. Xie, and F.N. Dang, "Experimental Study on the Mechanical Property and Damage Evolution of Concrete Under Freeze-thaw Environment", *Journal of Sichuan University(Engineering Science Edition)*, vol. 47, no. 04, pp. 38–44, 2015, DOI: 10.15961/j.jsuese.2015.04.006.

[26] Z.H. Guo, *Strength and Constitutive Relationship of Concrete-Principle and Application*. Beijing, China: China Architecture Publishing, 2004.

[27] K.Y. Cao, "Interpretation on the Paper of Quantitative Design of Frost Resistance of Concrete", *China Building Science Core Periodical*, no. 7, pp. 1–3, 2011, DOI: 10.3969/j.issn.1000-4637.2011.07.001.

[28] *ASTM C666/C666M-15 Standard Test Method for Resistance of Concrete to Rapid Freezing and Thawing*. ASTM International, 2015, DOI: 10.1520/C0666_C0666M-15.

Received: 2022-08-09, Received: 2022-11-29